



## Research Article

# Bioinspired tungsten-copper composites with Bouligand-type architectures mimicking fish scales

Yuan Zhang<sup>a,1</sup>, Guoqi Tan<sup>a,b,1</sup>, Mingyang Zhang<sup>a,b</sup>, Qin Yu<sup>c</sup>, Zengqian Liu<sup>a,b,\*</sup>, Yanyan Liu<sup>a,b</sup>, Jian Zhang<sup>a</sup>, Da Jiao<sup>a</sup>, Faheng Wang<sup>a,d</sup>, Longchao Zhuo<sup>e</sup>, Zhefeng Zhang<sup>a,b</sup>, Robert O. Ritchie<sup>c</sup>

<sup>a</sup> Shi-Changxu Innovation Center for Advanced Materials, Institute of Metal Research, Chinese Academy of Sciences, Shenyang 110016, China

<sup>b</sup> School of Materials Science and Engineering, University of Science and Technology of China, Hefei 230026, China

<sup>c</sup> Department of Materials Science and Engineering, University of California Berkeley, Berkeley, CA, 94720, USA

<sup>d</sup> Jihua Laboratory, Foshan 528200, China

<sup>e</sup> School of Materials Science and Engineering, Xi'an University of Technology, Xi'an 710048, China

## ARTICLE INFO

## Article history:

Received 16 January 2021

Revised 3 April 2021

Accepted 21 April 2021

Available online 2 June 2021

## Keywords:

Bouligand structure

Tungsten-copper composites

Fish scales

Structural reorientation

Bioinspired designs

## ABSTRACT

The microscopic Bouligand-type architectures of fish scales demonstrate a notable efficiency in enhancing the damage tolerance of materials; nevertheless, it is challenging to reproduce in metals. Here bioinspired tungsten-copper composites with different Bouligand-type architectures mimicking fish scales were fabricated by infiltrating a copper melt into woven contexts of tungsten fibers. These composites exhibit a synergetic enhancement in both strength and ductility at room temperature along with an improved resistance to high-temperature oxidation. The strengths were interpreted by adapting the classical laminate theory to incorporate the characteristics of Bouligand-type architectures. In particular, under load the tungsten fibers can reorient adaptively within the copper matrix by their straightening, stretching, interfacial sliding with the matrix, and the cooperative kinking deformation of fiber grids, representing a successful implementation of the optimizing mechanisms of the Bouligand-type architectures to enhance strength and toughness. This study may serve to promote the development of new high-performance tungsten-copper composites for applications, e.g., as electrical contacts or heat sinks, and offer a viable approach for constructing bioinspired architectures in metallic materials.

© 2021 Published by Elsevier Ltd on behalf of Chinese Society for Metals.

## 1. Introduction

The architectures of natural biological materials have been perfected through the long-term evolution of organisms and are now being increasingly regarded as blueprints to reproduce in man-made materials for enhanced performance [1–3]. The twisted plywood architecture, also known as Bouligand-type structure, is a prime example existing in a wide variety of natural materials like fish scales [4–8], arthropod cuticles [9–12], and vertebrate bones [13–15]. It features a periodically helicoidal stacking arrangement of stiff fibers or fiber bundles, comprising mineralized collagens for fish scales and bones, and chitins for arthropod cuticles, embedded within a less stiff matrix (typically of proteins). Such structures have been proven to be remarkably effective in enhancing

the damage tolerance of materials, especially under impact loading conditions; this is achieved by such processes as directing cracks to twist along the structure, accelerating the nucleation of microcracks without coalescence, and inducing the filtering effect of shear stress waves under impact [16–20]. In particular, the Bouligand-type structure can adapt to external loads principally by reorienting the fibers towards or away from the loading axis, respectively, in the case of tensile and compressive loading states [5,6,8,21]. Recently we have revealed that such mechanisms function, not merely as a passive response to allow for flexibility, but to effectively promote a simultaneous enhancement of the stiffness, strength, mechanical stability, and fracture toughness of materials [22,23].

The exceptional mechanical efficiency of the Bouligand-type structure is well exemplified by its two unique forms found in fish scales, as shown in Fig. 1(a–c). The first one features a microscopically orthogonal plywood structure where adjacent layers of fibers are rotated by 90° (Fig. 1(b)). Such a structure exists in the scales of many species of fish such as *Pagrus major* [4], *Morone sax-*

\* Corresponding authors.

E-mail addresses: [zengqianliu@imr.ac.cn](mailto:zengqianliu@imr.ac.cn) (Z. Liu), [zhfzhang@imr.ac.cn](mailto:zhfzhang@imr.ac.cn) (Z. Zhang), [roritchie@lbl.gov](mailto:roritchie@lbl.gov) (R.O. Ritchie).

<sup>1</sup> These authors contributed equally to this work.

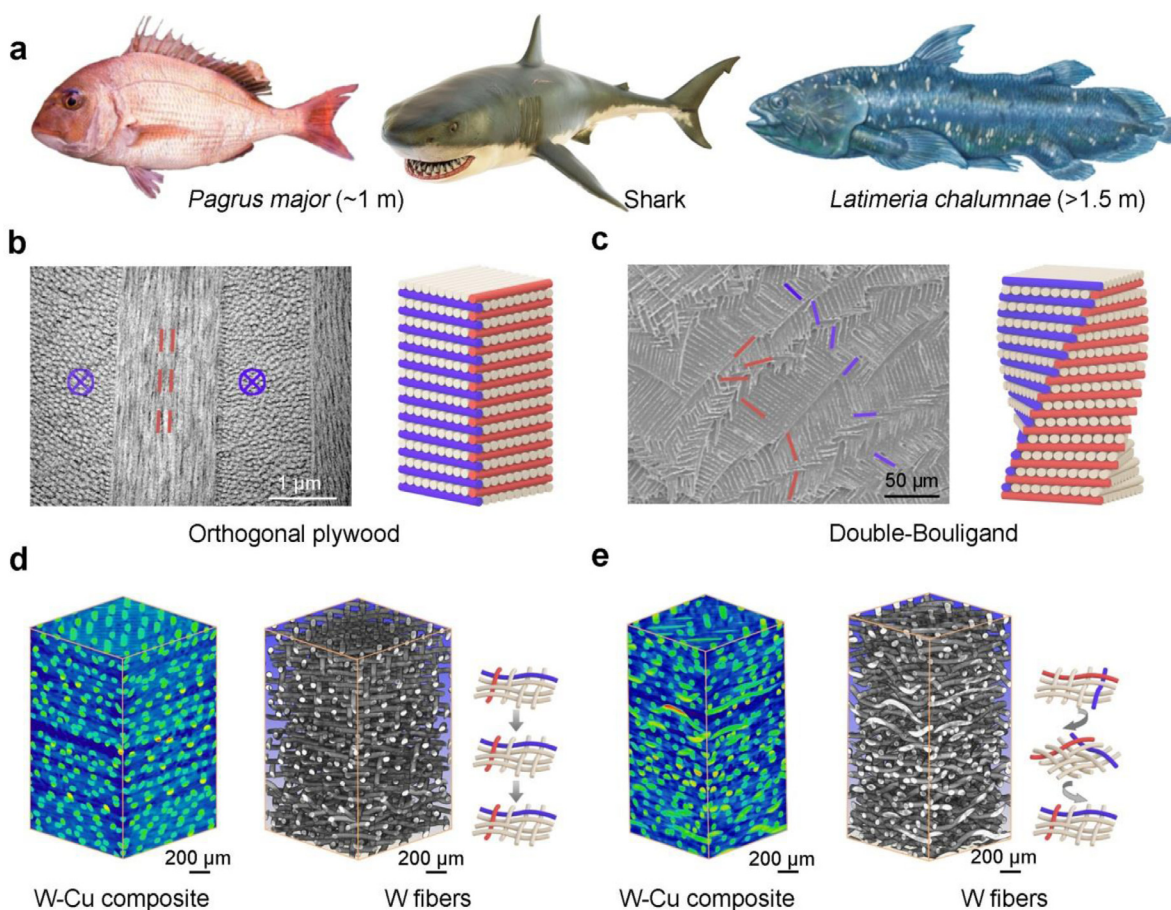


**Fig. 1.** Bouligand-type structures of bioinspired tungsten-copper composites mimicking fish scales. (a) The scales of *Pagrus major* and *Latimeria chalumnae* fish provide an effective protective role against the predation by sharks. (b, c) Micrographs and schematic illustrations of the orthogonal plywood and double-Bouligand structures in the scales of (b) *Pagrus major* and (c) *Latimeria chalumnae* fish. (d, e) 3-D microstructures of the tungsten-copper composites with bioinspired (c) orthogonal plywood and (d) double-Bouligand structures by XRT imaging. The spatial distributions of tungsten fibers within the composites are generated by filtering out the signals from the copper matrices. The micrographs of fish scales in (b) and (c) are adapted with permission from refs. [4,8].

*atilis* [24], *Poecilia reticulata* and *Hemichromis bimaculatus* [25]. The second form can be termed the double-Bouligand structure as its twisting unit comprises an orthogonal bilayer where the fibers are perpendicular to each other, *i.e.*, it is these bilayers that are helicoidally stacked following the Bouligand-type fashion (Fig. 1(c)). Such a structure has been observed in the scales of the African lung fish (*Protopterus annectens*) [26] and recently in the scales of the “living fossil” coelacanth fish (*Latimeria chalumnae*) [7,8]. It is clear that both the orthogonal plywood (single Bouligand) and double-Bouligand structures can lead to enhanced damage tolerance, thereby endowing the fish scales with effective protection. This is particularly evident by the fact that the large *Pagrus major* and *Latimeria chalumnae* fish can both grow to over 1 m in length, yet can survive in the shark infested waters [4,8] (Fig. 1(a)).

Bouligand-type structures have been replicated as a natural prototype in a range of man-made materials, including the polymer-matrix composites reinforced with carbon, glass or ceramic fibers, as well as the 3-D printed scaffolds of polymers, ceramics and even cement [20,27–33]. However, the constituents of these materials are generally brittle in nature which differs markedly from those in certain biological materials. As such, bioinspired Bouligand-type synthetic structures generally display limited to zero plasticity such that the involved fibers can hardly reorient in response to external loads. This makes it difficult to fully implement the adaptive structural reorientation mechanisms that enhance the properties of many of the natural structures [6,22]. Even if only an imitation of these structures is considered, it still

remains unclear how to choose and design the detailed configurations of orthogonal plywood and double-Bouligand structures to achieve the intended properties. Additionally, compared to the more common single-Bouligand structure, it has been shown that the double-Bouligand structure exhibits further improvements in toughening efficiency [18,34]. However, it is more challenging to replicate in man-made materials due to its higher level of structural complexity. Indeed, so far such structures have only been realized in 3-D printed polymeric model materials for verifying computational simulations [34]. Here we propose a bioinspired design protocol for implementing the underlying mechanisms for property optimization of Bouligand-type structures that mimic fish scales based on a ductile tungsten-copper composite system. The structure-property relationships are also elucidated for guiding the structural designs.

## 2. Experimental section

### 2.1. Composite fabrication

Commercially available tungsten meshes (Shengshida Materials Co., China) were employed as the twisting units for constructing the bioinspired Bouligand-type structures. These meshes comprise mutually perpendicular pairs of tungsten fibers which are interwoven together following an orthogonal configuration, as shown in Fig. S1 in the Supplementary Materials. The diameter and interspacing of the fibers were 50  $\mu\text{m}$  and 120–140  $\mu\text{m}$ , respec-

tively. The meshes were ultrasonically washed with 10% hydrofluoric acid (aqueous solution) to remove possible surface oxides, cleaned with ethanol, and then cut into pieces with 75 mm in diameter using scissors. These pieces were stacked layer-by-layer in differing modes to build the orthogonal plywood and double-Bouligand structures. Specifically, the orientations of the fibers were identical among layers for the orthogonal plywood structure, but were helically rotated by  $7.5^\circ$  between adjacent layers in an anticlockwise fashion for the double-Bouligand structure. It has been shown that a small twisting angle, generally less than  $10^\circ$ , is favorable for enhancing the damage tolerance of Bouligand-type structure [28,31,32]; nevertheless, it may lead to an unreasonably large thickness for each cycle of the helix. Here the twisting angle was determined as  $7.5^\circ$  such that two complete helical cycles could be generated in a lab-sized sample with a thickness of  $\sim 2.5$  mm, i.e., a total of 24 layers of tungsten meshes were contained. The stacked layers were then fixed using tungsten wires at their periphery and densified by pressing along the vertical direction at 50 MPa for 30 min.

Bioinspired composites were fabricated by pressureless infiltration of a copper melt into the stacks. This was accomplished by overlaying copper blocks on top of the stacks, heating them in flowing argon gas to  $1350^\circ\text{C}$  – some  $270^\circ\text{C}$  higher than the melting point of copper ( $1083^\circ\text{C}$ ) – and holding for 2 h followed by furnace cooling. For comparison, tungsten-copper composites were also prepared by sintering the compacts of mixed powders of tungsten (with a median diameter of  $1\ \mu\text{m}$ ) and copper (with a median diameter of  $50\ \mu\text{m}$ ) at  $900^\circ\text{C}$  for 2 h under a pressure of 20 MPa in flowing argon gas. These composites had similar compositions of constituents to the bioinspired ones (with a tungsten content of 26.8 vol.%), but exhibited a random structure featuring a uniform distribution of tungsten particles within the copper matrix.

## 2.2. Microstructural characterization

Scanning electron microscopy (SEM) imaging was performed using a LEO Supra-35 field-emission microscope (LEO, Germany) operating at an accelerating voltage of 20 kV. The through-thickness cross-sections of the infiltrated composites were ground and polished to a surface finish of  $\sim 0.5\ \mu\text{m}$  before observation. Oxidized samples, i.e., after thermogravimetric analysis or high-temperature tensile tests, were sputter-coated with a film of gold to reduce the charging effect. The 3-D structures of the composites were characterized by X-ray tomography (XRT) imaging using an Xradia Versa XRM-500 3-D X-ray microscope (Xradia, USA) operating at an accelerating voltage of 80 kV. A total of 1600 slices of 2-D projections were acquired for each sample and reconstructed to 3-D volume renderings based on the Fourier back-projection algorithm. The spatial resolution of the 3-D images was  $\sim 2.7\ \mu\text{m}$  per pixel. Image processing and analysis were conducted using the Avizo Fire 7.1 software (Visualization Sciences Group, France).

## 2.3. Mechanical testing

The Brinell hardness was measured on horizontal and vertical sections of the bioinspired composites, respectively parallel and perpendicular to the stacked layers of tungsten meshes, as illustrated in Fig. S2. Specifically, the vertical sections for the orthogonal plywood structure were parallel to the long axes of one set of the interwoven fibers. Measurements were performed using an XHB-3000 hardness tester (Everone Instrument, China) by pressing a tungsten carbide ball of 2.5 mm in diameter into samples polished to a surface finish of  $\sim 0.5\ \mu\text{m}$  with a load of 19 kg and a dwell time of 30 s, in accordance with the ISO 6506-1 Standard [35]. The indentation typically had a diameter of 1–1.5 mm which

far exceeded the interspacing of fibers so as to embody the full effects of the microstructure.

Room temperature tensile tests were conducted using an Instron 5982 testing machine (Instron Co., USA) at a strain rate of  $10^{-3}\ \text{s}^{-1}$  with the strain monitored using an Instron 2620-601 extensometer (Instron Co., USA). The samples had a gage dimension of  $13.5\ \text{mm} \times 6\ \text{mm} \times 2.5\ \text{mm}$  with their length directions conforming well to the basal planes of the stacked tungsten meshes for the bioinspired composites, as illustrated in Fig. S2. These samples were directly gripped onto the testing machine. Specifically, the tensile axis was parallel to the orientation of one set of fibers for the orthogonal plywood structure. The surfaces of samples were ground using sand paper up to 3000 grit before testing. The mechanical properties at elevated temperatures were evaluated by uniaxial tensile tests at  $800^\circ\text{C}$  in air using an MTS E45.105 testing machine (MTS, USA) at the same strain rate of  $10^{-3}\ \text{s}^{-1}$ . To avoid the occurrence of noticeable deformation in the samples caused by the gripping force due to the creep of the copper matrix, the samples for high-temperature tensile tests were clamped between two fixtures made of a superalloy. The gage dimension of the samples was restricted by these fixtures to be  $\sim 18\ \text{mm} \times 4\ \text{mm} \times 2.5\ \text{mm}$ . The loading configurations were consistent with those used for room temperature tests. A total of 24 layers of tungsten meshes were involved in all of the tensile samples through the thickness direction for the double-Bouligand structure to ensure the presence of two complete cycles of helices. At least three measurements were conducted for each set of samples.

## 2.4. Electrical conductivity measurement

The electrical conductivity of the composites was measured using a WD-Z eddy current conductivity meter (Hengxing, China). In view of the anisotropic nature of the bioinspired composites, the measurement was performed on both their horizontal and vertical sections where the induced eddy currents were parallel to and penetrated, respectively, the stacked layers of the tungsten meshes. The samples had a width and thickness of over 20 mm which far exceeded the diameter of the coil (10 mm). The surfaces of samples were ground and polished to a mirror finish before testing.

## 2.5. Thermogravimetric analysis

The high-temperature oxidation behavior of the composites was characterized by thermogravimetric analysis (TGA) using a Netzsch STA449F3 thermal analyzer (Netzsch, Germany). The measurements were performed at a heating rate of  $5^\circ\text{C}/\text{min}$  up to  $800^\circ\text{C}$  in flowing air with a flow rate of  $50\ \text{mL}/\text{min}$ , in accordance with the standards GB/T 13303-91 [36]. The samples were ground and polished to an identical dimension of  $13\ \text{mm} \times 7.4\ \text{mm} \times 1.8\ \text{mm}$  with a surface finish of  $\sim 0.5\ \mu\text{m}$  and ultrasonically cleaned with acetone before testing. The morphology of the oxidized samples was characterized by SEM.

## 2.6. Post-fracture characterization

The fractured tensile samples were also examined by SEM imaging. The 3-D configurations of the tungsten meshes within the composites were characterized by X-ray computed tomography (CT) using a YXLON CT Modular (YXLON International, Germany) operating at an accelerating voltage of 210 kV with a current of 0.1 mA. The 3-D volume renderings were reconstructed from a total of 2700 slices of 2-D projections around the samples, i.e., with the projections taken at an interval of 8 min. The spatial resolution for the 3-D images was  $\sim 11\ \mu\text{m}$  per pixel. This was lower than that for microstructural characterization by XRT imaging, but was high enough for discerning the orientations of tungsten fibers within

the composites. The CT images were processed and analyzed using the VGStudio Max software (Volume Graphics, Germany). To quantify the reorientation behavior, the fiber orientations in the two helices across the thickness direction of the samples were determined at their gage sections with a uniform elongation (necking was hardly discernable for the composites). At least 10 fibers with the same initial orientations were examined for each data point.

### 3. Results

#### 3.1. Bouligand-type architectures

Fig. 1 shows the 3-D microstructures of infiltrated tungsten-copper composites and their comparisons with the scales of *Pagrus major* and *Latimeria chalumnae* fish. It is seen that the naturally occurring Bouligand-type structures of fish scales can be effectively replicated in the composites based on the employment of different stacking modes of tungsten meshes. This is essentially represented by a layered arrangement of reinforcing tungsten fibers within a ductile copper matrix and the presence of specific orientation relationships between adjacent layers in line with the orthogonal plywood and double-Bouligand configurations (Fig. 1(d, e)). Such characteristics can be clearly illuminated by the serial slices of the 3-D views of the composites along their thickness direction, as shown in Movies S1 and S2. No obvious defects, e.g., voids or interfacial separation, were detected in the composites, indicating a full fill of the stacked meshes by a pressureless infiltration technique. The volume fractions of tungsten fibers were determined by X-ray tomography (XRT) to be ~26.8% and ~23.7%, respectively, for the composites with orthogonal plywood and double-Bouligand structures.

A key feature distinguishing the bioinspired composites from fish scales is that the orthogonal fibers are interwoven together within each layer unit in the composites, rather than being divided into individual sublayers containing unidirectional fibers as in fish scales [4–8]. This is presumed to favor improved intra-layer strength by preventing separation between the fibers. Such a design is reminiscent of the existence of inter-bundle fibers in the coelacanth fish scales which are arranged perpendicular to the layered structure and play a similar role by binding the fibers together [7,8,37].

#### 3.2. Enhanced mechanical properties

Fig. 2(a) shows representative room-temperature tensile stress-strain curves of the bioinspired composites and the overall appearance of the fractured samples. The results for the hot pressed sintered (PS) materials, which possess similar compositions but exhibit a uniform structure, are also presented for comparison. The sintered composites displayed a brittle fracture behavior at a low fracture stress of  $91 \pm 3$  MPa without exhibiting any detectable plasticity. Such poor mechanical properties are presumed to result from the presence of defects in the composites, e.g., in form of voids, impurities, and weak bonding between powders due to their surface oxide films, which is difficult to avoid with powder metallurgy processing [38]. In comparison, the bioinspired composites demonstrated a marked synergistic enhancement in both strength and ductility. Specifically, the ultimate tensile strengths were improved by a factor of ~3.5 and ~4.1, respectively, for the orthogonal plywood (OP) and double-Bouligand (DB) structures, as compared to the sintered materials. In particular, the composites with double-Bouligand structure can be continuously work hardened, leading to stable plastic deformation up to a strain of  $20 \pm 3\%$ .

The mechanical properties of the tungsten-copper composites were further evaluated at 800 °C in air in view of their potential high-temperature applications, e.g., as electrical contacts sub-

ject to arc erosion or as heat sinks in nuclear devices, where the instant temperatures can even approach 3000 °C [39–41]. A representatively high temperature of 800 °C was examined here for the bioinspired tungsten-copper composites; this temperature has also been commonly considered in the literature for materials of the same system [38,42–44]. As shown in Fig. 2(b), the sintered composites were consistently brittle at this temperature and exhibited ~35% lower strength than at room temperature. However, distinctly different mechanical properties were obtained for the bioinspired composites which depended on their specific configurations. Apparent yielding occurred at a low stress of ~10 MPa for the orthogonal plywood structure. This was followed by a clear work-hardening stage until fracture at  $58 \pm 4$  MPa, that generated a total ductility up to a strain of  $27 \pm 3\%$ . In contrast, the composites with a double-Bouligand structure displayed limited plasticity, with a fracture strain of  $4.8 \pm 1\%$ , but a higher strength of  $100 \pm 7$  MPa which was ~1.7 times than that of the uniform and orthogonal plywood structures.

#### 3.3. High-temperature oxidation behavior

The overall appearance of tensile fractured samples, shown in the inset in Fig. 2(b), suggests large differences in the high-temperature oxidation behavior between the bioinspired and sintered composites. It is noted here that the oxidation mainly occurs at the surface of the samples during the tensile tests at 800 °C, and specifically is limited to the outermost 1 or 2 layers of the tungsten meshes for the bioinspired composites. As such, the mechanical properties of the composites are still dominated by the unoxidized bulk and are closely associated with their structure. Fig. 2(c) presents the mass increase per unit surface area with temperature caused by oxidation, as measured by thermogravimetric analysis (TGA). It is seen that the onset temperatures for the sharp increase in mass, as indicated by the intersection points of tangent lines denoted by the arrows, were increased by ~50 °C for the bioinspired composites. This, combined with a lowered mass increase up to ~700 °C, clearly indicates an enhanced oxidation resistance. Such an attribute is deemed to result from the decrease in the volume density of interfaces between tungsten and copper which are generally preferential sites for oxidation [45]. A preliminary estimation, by respectively considering the morphologies of the tungsten phase as ideally cylindrical fibers and spherical powders for the bioinspired and sintered composites, gives an approximately one third decrease in the volume density of interfaces endowed by the bioinspired structures. As shown in the inset, the oxides were highly porous at the microscale and easily broken for the sintered samples (also shown in Fig. S3), whereas the surface layer remained intact as bonded by the less-oxidized tungsten meshes in the bioinspired composites. The slight mass decrease at the temperature range of 100–300 °C for the sintered samples, as indicated by the dashed arrow, may be caused by the formation of gaseous oxides from impurities, such as carbon.

#### 3.4. Hardness and electrical conductivity

The hardness and electrical conductivity of the bioinspired composites measured on different sections (detailed configurations are illustrated in Fig. S2) are presented in Fig. 2(d, e). Differing from the isotropic nature of the uniform structure, these properties are largely anisotropic in the bioinspired composites; nevertheless, their dependence on orientation is associated with the specific detailed configurations. Higher hardness and electrical conductivity were generated simultaneously on the vertical section for the composite with the double-Bouligand structure. In comparison, it was the horizontal section that was relatively harder but

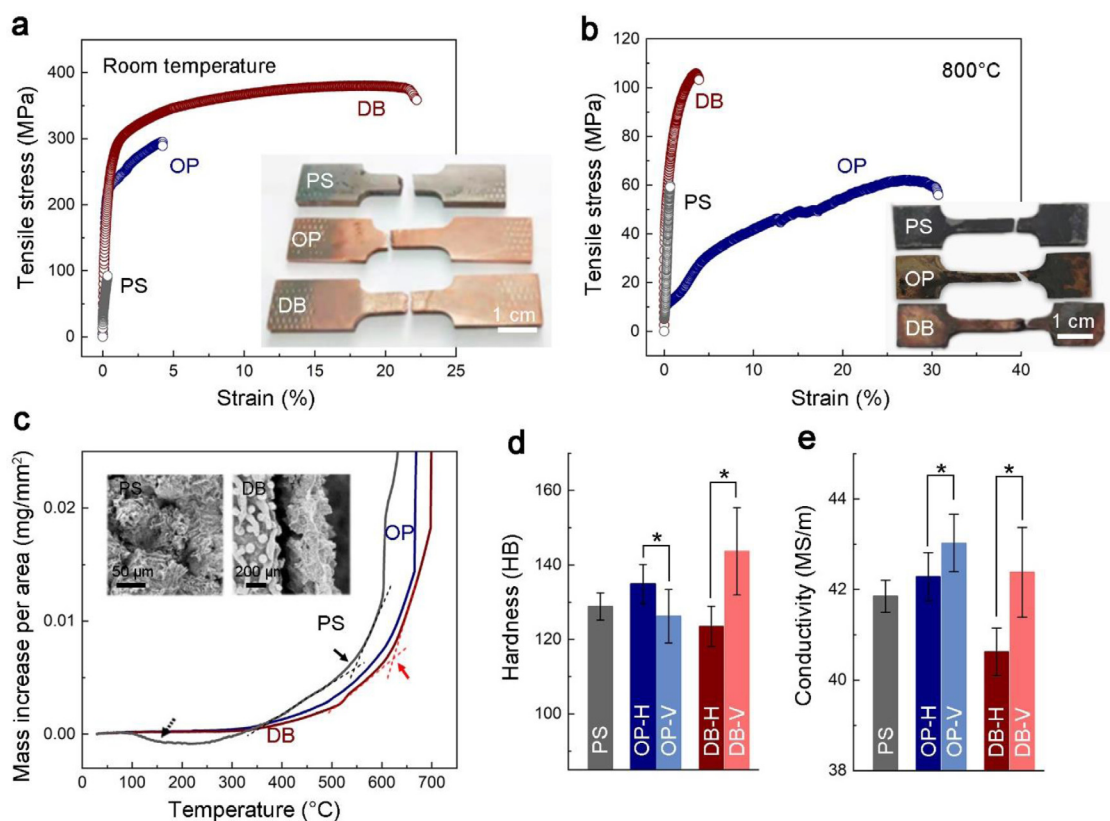


**Fig. 2.** Mechanical and functional properties of bioinspired tungsten-copper composites. (a, b) Representative tensile stress-strain curves for the bioinspired tungsten-copper composites with orthogonal plywood (OP) and double-Bouligand (DB) structures at (a) room temperature and (b) 800 °C as compared to the pressure sintered composites (PS) with a uniform structure. The overall appearances of the fractured samples are shown in the insets. (c) The mass increase per unit surface area of the composites with increasing temperature measured by TGA. Representative morphologies of the surface oxides for the sintered and bioinspired composites are shown in the insets. (d, e) Comparison of the (d) hardness and (e) electrical conductivity of the bioinspired composites measured on horizontal (H) and vertical sections (V) with those of the sintered samples. Asterisks indicate statistically significant differences at a 5% level of significance according to the Student's *t*-test.

exhibited lowered conductivity for the orthogonal plywood structure. The in-plane hardness, *i.e.*, on the vertical section, can be understood based on adapting classical laminate theory to incorporate the bioinspired Bouligand-type structures [46], as discussed below. The high electrical conductivity for the vertical section in both composites results principally from the easy penetration of current through the tungsten meshes across the wide interspacing between fibers, as shown in Fig. S1. By contrast, the dense compaction of these layers leads to narrow conduits for electrical conduction and thereby lower conductivities for the horizontal section. This is more evident for the double-Bouligand structure wherein the conduction paths exhibit increased complexity due to the helical twisting between layers.

### 3.5. Laminate theory modeling

Establishing the relationships between structure and mechanical properties in bioinspired composites could provide theoretical basis for guiding their structural design to achieve intended properties. To this end, classical laminate theory [46] was adapted here for the bioinspired structures by treating individual lamina as structural unit and incorporating the orientation relationships between adjacent laminae. By this means, the effects of different bioinspired Bouligand-type structures with the orthogonal plywood and double-Bouligand configurations were incorporated to interpret room temperature mechanical properties. The orthogonal plywood structure can be seen as a special case of the double-Bouligand structure with the twisting angle between adjacent bilayers equal to 0° or 90°. Our analysis considered a thin lamina

comprising perfectly bonded laminae such that the inter-lamina shear deformation can be ignored [46,47]. This assumption is in line with the experimental results where no obvious slippage between tungsten meshes could be detected. The laminate consists of a total of 24 laminae through its thickness direction; each lamina represents a composite layer containing a bilayer of orthogonal fibers with an identical thickness  $t_0$ . These laminae, numbered in sequence from the bottom to the top, are twisted in an anti-clockwise manner with a pitch angle  $\varphi$ , forming a balanced antisymmetric conformation, *i.e.*, the upper and lower laminae are at an equal  $z$ -distance from the mid-plane and exhibit opposite rotations. These structural characteristics are fully consistent with those in the experiments.

Fig. 3(a) illustrates the local coordinate system (1,2) for individual lamina and the global coordinate system ( $x,y$ ) for the entire laminate, both of which are right-handed. The principal axes 1 and 2 for each lamina were defined to be parallel and perpendicular, respectively, to one fixed set of interwoven fibers. Indeed, these axes are essentially equivalent within the individual lamina for the orthogonal bilayer. The coordinate of the laminate coincides with that of the mid-plane which can be determined using the bisectors of the principal axes of the 12th and 13th laminae. In this scenario, the structural orientation and position of the  $k^{\text{th}}$  lamina can be described as follows:

$$\theta_k = (k - 12.5)\varphi,$$

$$z_k = (k - 12)t_0, \quad (1)$$

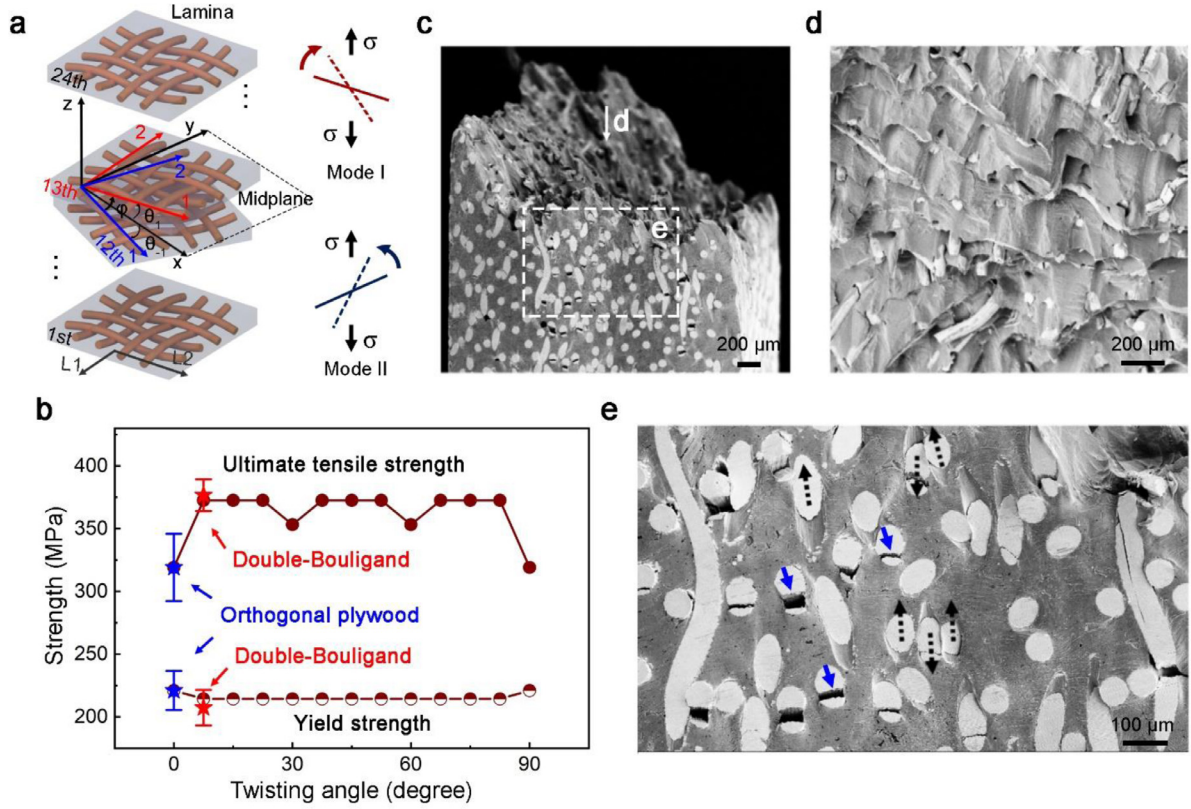


**Fig. 3.** Interpretation of the mechanical properties for the bioinspired Bouligand-type structures. (a) Schematic illustrations of the laminate composite model and coordinate system for the theoretical analysis, and the definition of the two different reorientation modes (I and II) of tungsten fibers in the composite. (b) Theoretical results on the variations in the yield and ultimate tensile strengths of the entire laminate as a function of the twisting angle between adjacent laminae for the bioinspired double-Bouligand structure (the twisting angle equals 0° for the orthogonal plywood structure). Experimental data are presented for comparison. (c–e) SEM micrographs of a fractured sample for the composite with the double-Bouligand structure after tensile testing at room temperature. (d) and (e) show the magnified views for the fracture surface and lateral profile, respectively, of the sample as indicated by the arrow and dashed box in (c).

where  $\theta_k$  and  $z_k$  are, respectively, the rotation angle and  $z$ -distance of the lamina with respect to the mid-plane.

Considering the loading configuration ( $L_1, L_2$ ) where  $L_1$  conforms to the 1 axial direction of the fibers in the 1st lamina, the principal forces  $\sigma$  and moments  $m$  of the laminate, both normalized by the area, or equivalently thickness, of the model with its length and width set as unity, can be correlated to the in-plane strains  $\epsilon_0$  and curvatures  $\kappa$  following the relationship [46,47]:

$$\begin{bmatrix} \sigma \\ m \end{bmatrix} = \begin{bmatrix} \mathbf{A} & \mathbf{B} \\ \mathbf{B} & \mathbf{D} \end{bmatrix} \begin{bmatrix} \epsilon_0 \\ \kappa \end{bmatrix}. \quad (2)$$

Vectors are used here for all the parameters to encompass the different components in the  $x$ ,  $y$  and  $xy$  directions.  $\mathbf{A}$ ,  $\mathbf{B}$  and  $\mathbf{D}$  are the stiffness matrices for the stress-states of extension, extension-bending coupling and bending, which are given by:

$$\begin{aligned} \mathbf{A} &= \frac{1}{2nt_0} \sum_{k=1}^{2n} [\mathbf{Q}_k(z_k - z_{k-1})], \\ \mathbf{B} &= \frac{1}{4nt_0} \sum_{k=1}^{2n} [\mathbf{Q}_k(z_k^2 - z_{k-1}^2)], \\ \mathbf{D} &= \frac{1}{6nt_0} \sum_{k=1}^{2n} [\mathbf{Q}_k(z_k^3 - z_{k-1}^3)], \end{aligned} \quad (3)$$

where  $n$  is half the number of laminae in the laminate which equals 12.  $\mathbf{Q}_k$  is the stiffness matrix for the  $k^{\text{th}}$  lamina obtained by transforming the lamina stiffness matrix from its local coordinate (1,2) to the principal axes of laminate ( $x, y$ ) using the rotation

angle  $\theta_k$ . Specifically, Eqs. (2) and (3) provide a fundamental basis for correlating the structural characteristics to mechanical properties in bioinspired composites with Bouligand-type structures.

The Young's modulus and strength of the entire laminate can then be obtained from those of the individual lamina for different bioinspired Bouligand-type structures. Specifically, the fiber orientations in the orthogonal bilayers are all consistent for the orthogonal plywood structure. As such, the mechanical properties of the individual lamina along their principal axes can be determined using those of the orthogonal plywood composite which were measured experimentally. In addition, considering the dependences of strengths on the orientations for the orthogonal bilayers, the yielding of the entire laminate can be seen to be the result of the failure of the first lamina, *i.e.*, the lamina with the lowest strength. In this scenario, the conservative first-ply failure criterion [46,48], *i.e.*, using the critical stress at which the first lamina fails, was used to assess the yield strength of the composites. Similarly, the ultimate tensile strength was evaluated using the critical stress at which all the laminae fail, *i.e.*, corresponding to the failure of the final lamina [46]. Full details of this derivation are described in the Supplementary Materials.

Fig. 3(b) presents the variations of the yield and ultimate tensile strengths of the laminate as a function of the twisting angle for the bioinspired Bouligand-type structures. The theoretical results on the Young's modulus and their comparison with experimental data are presented in Fig. S4. Here only the angles that are exactly divisible by 90° were considered to ensure the presence of full cycles of helices. It is seen that the strength and Young's modulus of the current orthogonal plywood and double-Bouligand compos-

ites, *i.e.*, with twisting angles equaling  $0^\circ$  and  $7.5^\circ$  respectively, can be well described by the theoretical analysis. A key mechanical attribute of the double-Bouligand structure, as compared to the orthogonal plywood one, is that it can lead to lower yield strength but simultaneously higher ultimate tensile strength. This is different from the general scenario in metallic materials where these two properties often display similar varying trends [49].

### 3.6. Fracture characteristics

The marked enhancement in the room temperature ductility for the double-Bouligand structure is strongly associated with the coordinated deformation and the delocalization of damage between layers with different fiber orientations. As shown in Fig. 3(c), the global fracture profile presents a twisted curved shape involving two helices, which is in line with the structure. At the microscale, the fracture surface features a rough staircase-like morphology with each stair corresponding to a layer of tungsten meshes (Fig. 3(d)). This suggests that the local damage processes, such as fiber fracture and pull-out from the matrix, are not concentrated into the same plane, but instead exhibit a wide distribution among different layers. The magnified view of one entire helix, shown in Fig. 3(e), demonstrates notable differences in the deformation behavior of tungsten fibers with differing orientations. Specifically, the fibers parallel to the tensile direction became straightened and stretched until fracture, whereas axial splitting was more evident in the nearly perpendicular fibers, as indicated by the solid arrows. Interfacial slippage between the fibers and matrix occurred for the fibers with an oblique alignment with respect to the loading axis. Nevertheless, the direction and extent of the slip deformation differ depending largely on the fiber orientations, as exemplified by the dashed arrows. Such mixed modes of deformation and damage are considered to favor a stable tensile ductility by impeding gross fracture caused by the dominance of any of these factors.

In contrast, the mechanical behavior of the composite with the orthogonal plywood structure is governed by the successive straightening, stretching and fracture of the axial fibers and their pull-out from the matrix, as shown in Fig. S5. The fibers perpendicular to the loading direction are easy to separate from each other and as such contribute slightly to the strength and work-hardening ability. Therefore, the enhanced strengthening efficiency of the double-Bouligand structure is closely associated with the participation of fibers with different orientations in the deformation. Such an effect is more prominent at elevated temperatures where the fracture of the composite necessitates the breakage of almost all these fibers (Fig. S6). The extensive plasticity involved with the orthogonal plywood structure at  $800^\circ\text{C}$  is believed to result from the continuous pull-out of fractured fibers from the copper matrix which displays creep behavior at a low stress level (Fig. S5).

### 3.7. Adaptive structural reorientation

The 3-D X-ray CT images of the room temperature fractured samples, shown in Fig. 4(a), reveal an obvious shape change and extension of the grids of tungsten meshes in the composite with the double-Bouligand structure. The deviation of the inclination angle between interwoven fibers from  $90^\circ$  clearly indicates a change in their orientations during the deformation process, which is reminiscent of the adaptive structural reorientation behavior of fish scales [5,6,22,23]. The differing geometries of the grids along the thickness direction of composite imply that the extent of such reorientation is closely associated with the initial orientations of the fibers. The reorientation angles, *i.e.*, the changes in the inclination of the fibers with respect to the loading axis, are defined

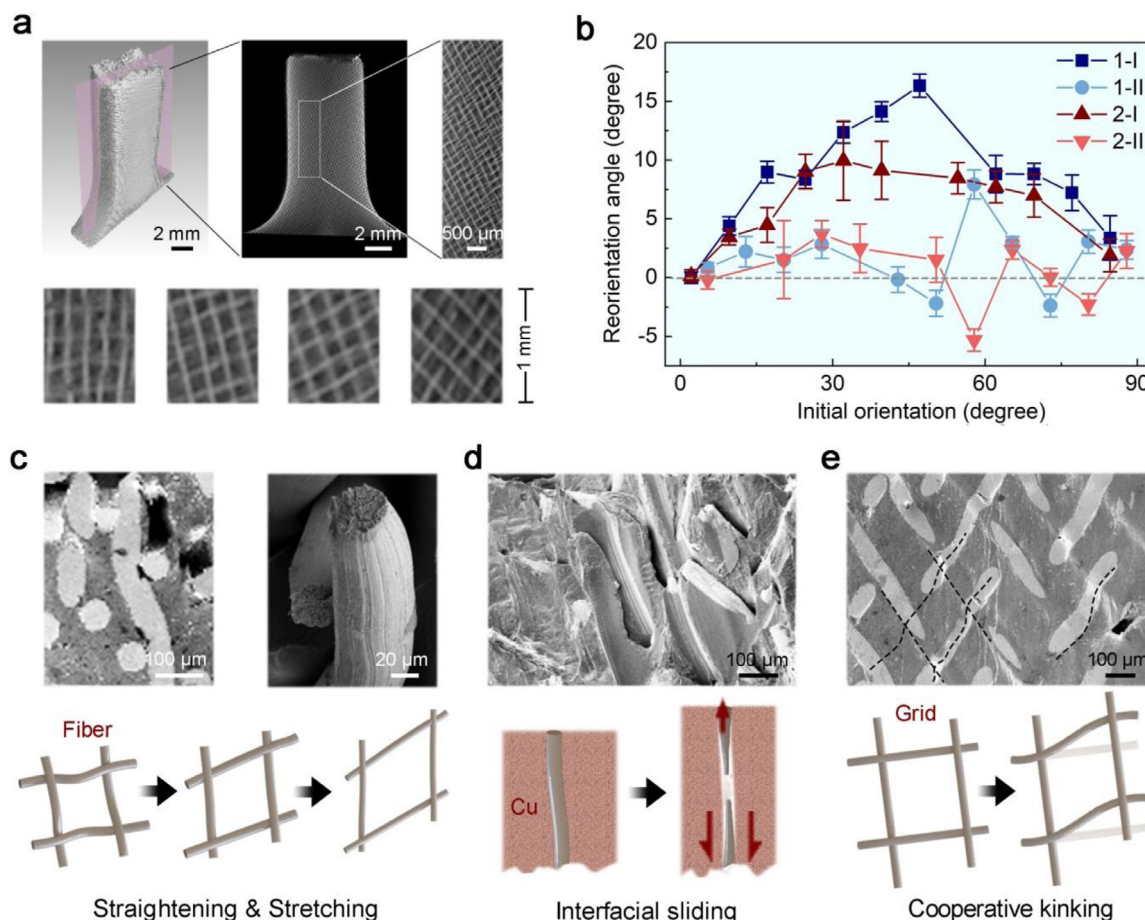
as positive when the fibers are rotated towards the tensile loading direction, which is most common in natural materials [5,6,22,23]. There are two distinctly different modes for the structural reorientation. As illustrated in Fig. 3(a), the rotation of fibers is principally in a clockwise fashion when the initial inclination angles of their 1 axes are positive with respect to the loading axis L1 according to the right-hand rule (mode I). On the contrary, the majority of fibers with initially negative orientations are rotated in an anti-clockwise fashion (mode II). The difference between the two modes lies essentially in the relationship between the principal rotation directions for reorientation of the tungsten fibers and their original twisting directions for arrangement in the composites. The principal reorientation directions are consistent with the original twisting directions for mode I; conversely, the two directions are opposite for mode II.

Fig. 4(b) presents the variations in the reorientation angles of tungsten fibers as a function of their initial orientations (with all parameters depicted using their absolute values). It is seen that the mode I reorientation is continuously enhanced with increasing inclination of the fibers with respect to the external load, and then decreases to a minimum when the fibers are nearly perpendicular to the loading axis. A peak value of up to more than  $15^\circ$  can be generated for the reorientation angle at an initial orientation of around  $45^\circ$  where the fiber alignment conforms exactly to the plane with the maximum shear stress. This is consistent with the varying trend observed in the coelacanth fish scales where oblique fibers tend to exhibit obvious reorientation [5,6]. Nevertheless, the reorientation angles in the current composites are larger than those for the mineralized collagen fibers in fish scales which rarely exceed  $10^\circ$ . In contrast, the mode II reorientation of the tungsten fibers is much less evident over the entire range of initial orientations. The different reorientation behavior between mode I and II is deemed to result from the marked difference in their resistance to fiber rotation. Specifically, the “back” rotation of fibers towards the tensile direction, against their twisting arrangement for mode II, confronts a higher level of constraint from adjacent tungsten meshes; it is therefore inhibited and may even display negative reorientation angles.

The adaptive reorientation of tungsten fibers within the copper matrix originates from a series of mechanisms at the microscale. As shown in Fig. 4(c), the straightening of the originally curved fibers and their stretching deformation could promote the rotation of their long axes towards the tensile direction. Another important factor is the interfacial sliding between the fibers and matrix (Fig. 4(d)). This is particularly noticeable in view of the pull-out movement of fractured fibers from the matrix, as manifested by the resultant deep pits on the fracture surface. Additionally, the interwoven fibers display a cooperative kinking behavior evidenced by the tiny steps on the surface of samples, as indicated by the dashed curves in Fig. 4(e). Macroscopic reorientation can be produced because of the accumulation of the micro-buckling deformation of fibers at these steps. It is noted that the good plastic deformability of the copper matrix plays a key role in avoiding the premature fracture of these composites, thereby allowing for the stable reorientation of fibers.

## 4. Discussion

With respect to the manufacture of these materials, there are invariably considerable difficulties in constructing bioinspired structures with metallic materials due to their stringent processing conditions, *e.g.*, the need for high temperatures and large-scale deformation. This is especially the case for the Bouligand-type structures which to date have rarely been replicated in a synthetic metallic material. The current protocol of infiltrating contextures of woven fibers with a melt, however, does offer a viable approach



**Fig. 4.** Adaptive structural reorientation behavior of the bioinspired tungsten-copper composites. (a) X-ray CT images of a fractured sample after tensile testing at room temperature showing a clear shape change and extension of the grids of tungsten meshes in the composite with the bioinspired double-Bouligand structure. (b) Variations in the reorientation angle of the tungsten fibers following the different modes (I and II) as a function of their initial orientations with respect to the loading axis. The numbers 1 and 2 denote the two different cycles of helices in the composites. (c–e) Schematic illustrations and the corresponding experimental verification based on SEM characterization concerning the micro-mechanisms for adaptive structural reorientation.

for addressing this challenge. In particular, the structural characteristics of the resultant bioinspired composites can be intentionally designed and are easily adjustable by controlling the weaving method of the fibers. Indeed, woven meshes with different configurations are commercially available for a wide variety of metals and alloys. There are two basic requirements for the application of the melt infiltration technique: (1) the melting points of the reinforcing contexts must be markedly higher than those of the matrices, and (2) no severe chemical reactions or solubility must occur at the melting temperatures of the matrices. These can be fulfilled in a range of metallic systems, especially those involving refractory reinforcements, e.g., tungsten-copper and niobium-copper [38,42–44,50], or matrices with low melting points, e.g., titanium-magnesium and Nitinol-magnesium [51,52].

With respect to the mechanical properties, the coordinated deformation of the tungsten fibers with different orientations and their adaptive reorientation within the copper matrix endow the composites with notable work-hardening ability, specifically for the double-Bouligand structure at room temperature. The damage can also be delocalized among the tungsten layers owing to their twisting arrangement. As such, a high strength with large stable plastic deformation can be generated. However, the above mechanisms are absent for the orthogonal plywood structure where the easy separation between the fibers that are perpendicular to the tensile direction leads to lowered strengthening efficiency. At 800 °C, how-

ever, the failure of the composites is principally governed by creep deformation in the copper matrix. For the orthogonal plywood structure, the strengthening effect of the fibers that are parallel to the tensile direction can be dramatically reduced due to their easy straightening and slippage within the copper matrix. This along with the stretching of these fibers to breakage and their subsequent pull-out from the matrix leads to a large elongation. By contrast, for the double-Bouligand structure, almost all the fibers can play a strengthening role and are inhibited from slippage and pull-out within the matrix owing to their different orientations. This endows the composite with markedly higher strength than the orthogonal plywood structure but at a compromise with the elongation. Therefore, the double-Bouligand structure should be more favorable for high-temperature applications where the strength or creep resistance, instead of plasticity, is usually a major concern. Additionally, at room temperature the copper matrix exhibits a relatively high strength and thereby can help lower the stress in the tungsten fibers. However, the applied stress is principally concentrated in the fibers at 800 °C due to the obvious weakening of matrix. For the composite with the double-Bouligand structure, this leads to the fracture of fibers at a limited elongation which is markedly smaller than at room temperature.

The clarification of the structure-property relationships by adapting the classical laminate theory may provide insights into the mechanical role of Bouligand-type structures with different

configurations. In particular, only half the number of laminae is required to construct a full cycle of helix for the double-Bouligand structure, as compared to the more common single-Bouligand structure considering an equal twisting angle. This makes it more efficient for building materials with reduced thickness. Additionally, the double-Bouligand structure endows the tungsten-copper composite with a marked in-plane isotropy of mechanical properties along with improved oxidation resistance at high temperatures. This is realized at only a slight compromise with a decrease of strength by ~50 MPa than the unidirectional fiber-reinforced composites [53,54]. It is believed that these properties can be further optimized by regulating the structural characteristics. By such means, the bioinspired Bouligand-type structures demonstrate a good potential for generating enhanced performance in engineering materials.

A unique advantage distinguishing the Bouligand-type structures from other designs in biological materials is that they allow for the adaptive structural reorientation of reinforcing fibers during deformation [5,6]. We believe that such a mechanism paves the way for a new approach for creating the simultaneous optimization of a variety of nominally mutually exclusive properties, e.g., strength vs. toughness and stiffness vs. flexibility [22,23] by defeating the general “conflicts” between them. However, the bioinspired composites with Bouligand-type structures reported to date rarely display similar reorientation behavior because of the brittle nature of their constituents [20,27–32]. In the present study, it is clear that the plasticity of the copper matrix and the interwoven structure of tungsten fibers are vital for activating the multiple micro-mechanisms (Fig. 4(c-e)), thereby bestowing a good adaptability which is even more pronounced than in natural fish scales. We emphasize that this represents more than a simple replication of the naturally occurring structures but an implementation of the key optimizing mechanisms behind them which is the essence of bioinspired designs.

## 5. Conclusions

High-temperature bioinspired tungsten-copper composites with Bouligand-type structures that mimic fish scales were fabricated by pressureless infiltration of woven textures of tungsten fibers with a copper melt. These composites demonstrated a notable enhancement of mechanical properties and oxidation resistance up to 800 °C as compared to the sintered ones with a uniform structure. Specifically, the strength and ductility were simultaneously improved at room temperature, whereas at elevated temperatures high strength and good ductility were obtained, respectively, for the double-Bouligand and orthogonal plywood structures. The mechanical properties were interpreted by adapting classical laminate theory to different configurations for the Bouligand-type structures. The double-Bouligand structure was found to be the most effective in achieving a high ultimate tensile strength with a concurrent large ductility by promoting coordinated deformation, delocalizing local damage, and inducing crack twisting between layers with varying orientations. In particular, the tungsten fibers can reorient adaptively to a large extent within the copper matrix during the deformation process of the composites, indicating a successful implementation of the optimizing mechanisms of Bouligand-type structures in enhancing strength and toughness. This was enabled by the activation of a series of mechanisms at the microscale, including the straightening and stretching of tungsten fibers, the interfacial sliding between fibers and matrix, and the cooperative kinking deformation of fiber grids. This study may offer guidance for the bioinspired design of Bouligand-type structures and promote their applications in engineering materials for generating enhanced performance.

## Data availability

The data that support the findings of this study are available from the corresponding author, Prof. Zengqian Liu, at zengqian-liu@imr.ac.cn, upon reasonable request.

## Declaration of Competing Interests

The authors declare no conflict of interest.

## Acknowledgements

The authors are grateful for the financial support by the National Key R&D Program of China under grant number 2020YFA0710404, the National Natural Science Foundation of China under grant number 51871216, the KC Wong Education Foundation (GJTD-2020-09), the Liaoning Revitalization Talents Program, the State Key Laboratory for Modification of Chemical Fibers and Polymer Materials at Donghua University, the Opening Project of Jiangsu Province Key Laboratory of High-End Structural Materials under grant number hsm1801, and the Youth Innovation Promotion Association CAS. ROR acknowledges support from the Multidisciplinary University Research Initiative to University of California Riverside, funded by the Air Force Office of Scientific Research (AFOSR-FA9550-15-1-0009) and subcontracted to the University of California Berkeley.

## Supplementary materials

Supplementary material associated with this article can be found, in the online version, at doi:10.1016/j.jmst.2021.04.022.

## References

- [1] M.A. Meyers, J. McKittrick, P.Y. Chen, *Science* 339 (2013) 773–779.
- [2] S.J. Ling, D.L. Kaplan, M.J. Buehler, *Nat. Rev. Mater.* 3 (2018) 1–15.
- [3] F. Barthelat, Z. Yin, M.J. Buehler, *Nat. Rev. Mater.* 1 (2016) 1–16.
- [4] T. Ikoma, H. Kobayashi, J. Tanaka, D. Walsh, S. Mann, *J. Struct. Biol.* 142 (2003) 327–333.
- [5] W. Yang, V.R. Sherman, B. Gludovatz, M. Mackey, E.A. Zimmermann, E.H. Chang, E. Schaible, Z. Qin, M.J. Buehler, R.O. Ritchie, M.A. Meyers, *Acta Biomater.* 10 (2014) 3599–3614.
- [6] E.A. Zimmermann, B. Gludovatz, E. Schaible, N.K.N. Dave, W. Yang, M.A. Meyers, R.O. Ritchie, *Nat. Commun.* 4 (2013) 1–7.
- [7] M.M. Giraud, J. Castanet, F.J. Meunier, Y. Bouligand, *Tissue Cell* 10 (1978) 671–686.
- [8] H. Quan, W. Yang, E. Schaible, R.O. Ritchie, M.A. Meyers, *Adv. Funct. Mater.* 28 (2018) 1804237.
- [9] S. Nikolov, M. Petrov, L. Lympirakis, M. Friák, C. Sachs, H.O. Fabritius, D. Raabe, J. Neugebauer, *Adv. Mater.* 22 (2010) 519–526.
- [10] A. Al-Sawalmih, C. Li, S. Siegel, H. Fabritius, S. Yi, D. Raabe, P. Fratzl, *O. Paris, Adv. Funct. Mater.* 18 (2008) 3307–3314.
- [11] R. Yang, A. Zaheri, W. Gao, C. Hayashi, H.D. Espinosa, *Adv. Funct. Mater.* 27 (2017) 1603993.
- [12] J. Zhang, G. Tan, M. Zhang, D. Jiao, Y. Zhu, S. Wang, Z. Liu, D. Liu, Z. Zhang, *J. Mech. Behav. Biomed. Mater.* 91 (2019) 278–286.
- [13] M.M. Giraud-Guille, *Calcif. Tissue Int.* 42 (1988) 167–180.
- [14] W. Wagermaier, H.S. Gupta, A. Gourrier, M. Burghammer, P. Roschger, P. Fratzl, *Biointerphases* 1 (2006) 1–5.
- [15] S. Weiner, W. Traub, H.D. Wagner, *J. Struct. Biol.* 126 (1999) 241–255.
- [16] N. Guarrín-Zapata, J. Gomez, N. Yaraghi, D. Kisailus, P.D. Zavattieri, *Acta Biomater.* 23 (2015) 11–20.
- [17] F.D. Fischer, O. Kolednik, J. Predan, H. Razi, P. Fratzl, *Acta Biomater.* 55 (2017) 349–359.
- [18] Z. Song, Y. Ni, S. Cai, *Acta Biomater.* 91 (2019) 284–293.
- [19] N. Suksangpanya, N.A. Yaraghi, D. Kisailus, P. Zavattieri, *J. Mech. Behav. Biomed. Mater.* 76 (2017) 38–57.
- [20] N. Suksangpanya, N.A. Yaraghi, R.B. Pipes, D. Kisailus, P. Zavattieri, *Int. J. Solids Struct.* 150 (2018) 83–106.
- [21] J. Keckes, I. Burgert, K. Frühmann, M. Müller, K. Kölln, M. Hamilton, M. Burghammer, S.V. Roth, S. Stanzi-Tschegg, P. Fratzl, *Nat. Mater.* 2 (2003) 810–813.
- [22] Z. Liu, Y. Zhang, M. Zhang, G. Tan, Y. Zhu, Z. Zhang, R.O. Ritchie, *Acta Biomater.* 86 (2019) 96–108.
- [23] Z. Liu, Z. Zhang, R.O. Ritchie, *Adv. Funct. Mater.* 30 (2020) 1908121.
- [24] D. Zhu, C.F. Ortega, R. Motamedi, L. Szewciw, F. Vernerey, F. Barthelat, *Adv. Eng. Mater.* 14 (2012) B185–B194.

- [25] L. Zylberberg, J. Bereiter-Hahn, J.Y. Sire, *Cell Tissue Res.* 253 (1988) 597–607.
- [26] L. Zylberberg, *J. Zool.* 216 (1988) 55–71.
- [27] L.K. Grunenfelder, N. Suksangpanya, C. Salinas, G. Milliron, N. Yaraghi, S. Herrera, K. Evans-Lutterodt, S.R. Nutt, P. Zavattieri, D. Kisailus, *Acta Biomater.* 10 (2014) 3997–4008.
- [28] J.L. Liu, H.P. Lee, V.B.C. Tan, *Compos. Sci. Technol.* 165 (2018) 282–289.
- [29] K. Wu, Z. Song, S. Zhang, Y. Ni, S. Cai, X. Gong, L. He, S. Yu, *Proc. Natl. Acad. Sci. U. S. A.* 117 (2020) 15465–15472.
- [30] M. Moini, J. Olek, J.P. Youngblood, B. Magee, P.D. Zavattieri, *Adv. Mater.* 30 (2018) 1802123.
- [31] S. Yin, H. Chen, R. Yang, Q. He, D. Chen, L. Ye, Y. Mai, J. Xu, R.O. Ritchie, *Cell Rep. Phys. Sci.* 1 (2020) 100109.
- [32] L. Cheng, A. Thomas, J.L. Glancey, A.M. Karlsson, *Composites, Part A* 42 (2011) 211–220.
- [33] Z. Sun, T. Liao, W. Li, Y. Dou, K. Liu, L. Jiang, S. Kim, J. Kim, S. Dou, *NPG Asia Mater.* 7 (2015) e232.
- [34] S. Yin, W. Yang, J. Kwon, A. Wat, M.A. Meyers, R.O. Ritchie, *J. Mech. Phys. Solids* 131 (2019) 204–220.
- [35] *Metallic Materials – Brinell Hardness Test – Part 1: Test method*, European Committee for Standardization, 2005.
- [36] G.B./T. 13303-1991, *Steels – Determination Method of Oxidation Resisitance*, China Standard Press, 1991.
- [37] V.R. Sherman, H. Quan, W. Yang, R.O. Ritchie, M.A. Meyers, *J. Mech. Behav. Biomed. Mater.* 73 (2017) 1–16.
- [38] H. Abbaszadeh, A. Masoudi, H. Safabinesh, M. Takestani, *Int. J. Refract. Met. Hard Mater.* 30 (2012) 145–151.
- [39] M. Ahangarkani, K. Zangeneh-Madar, S. Borji, Z. Valefi, *Int. J. Refract. Met. Hard Mater.* 67 (2017) 115–124.
- [40] W. Chen, L. Dong, Z. Zhang, H. Gao, J. Mater. Sci.: Mater. Electron. 27 (2016) 5584–5591.
- [41] L. Dong, M. Ahangarkani, W. Chen, Y. Zhang, *Int. J. Refract. Met. Hard Mater.* 75 (2018) 30–42.
- [42] E. Tejado, A. Müller, J.-H. You, J. Pastor, *J. Nucl. Mater.* 498 (2018) 468–475.
- [43] A.G. Hamidi, H. Arabi, S. Rastegari, *Int. J. Refract. Met. Hard Mater.* 29 (2011) 538–541.
- [44] A.v. Müller, D. Ewert, A. Galatanu, M. Milwich, R. Neu, J.Y. Pastor, U. Siefken, E. Tejado, J.H. You, *Fusion Eng. Des.* 124 (2017) 455–459.
- [45] R.J. Kerans, R.S. Hay, T.A. Parthasarathy, M.K. Cinibulk, *J. Am. Ceram. Soc.* 85 (2002) 2599–2632.
- [46] R.M. Jones, *Mechanics of Composite Materials*, CRC Press, Philadelphia, USA, 2014.
- [47] I. Greenfeld, I. Kellersztein, H.D. Wagner, *Nat. Commun.* 11 (2020) 1–12.
- [48] Y. Li, S. Pimenta, *Compos. Struct.* 209 (2019) 1005–1021.
- [49] M.A. Meyers, K.K. Chawla, *Mechanical Behavior of Materials*, Cambridge University Press, Cambridge, UK, 2008.
- [50] Y. Zhang, G. Tan, D. Jiao, J. Zhang, S. Wang, F. Liu, Z. Liu, L. Zhuo, Z. Zhang, S. Deville, R.O. Ritchie, *J. Mater. Sci. Technol.* 45 (2020) 187–197.
- [51] S.F. Hassan, M. Gupta, *J. Alloys Compd.* 345 (2002) 246–251.
- [52] M. Zhang, Q. Yu, Z. Liu, J. Zhang, G. Tan, D. Jiao, W. Zhu, S. Li, Z. Zhang, *R. Yang, Sci. Adv.* 6 (2020) eaba5581.
- [53] V.S. Ivanova, L.M. Ustinov, Y.E. Busalov, V.G. Gvozdyk, *Strength Mater* 1 (1969) 278–282.
- [54] M. Bomford, A. Kelly, *Fibre Sci. Technol.* 4 (1971) 1–8.